Water remediation capability of cubic-phase CdS nanoparticles as photocatalyst on photodegradation of aqueous rhodamine 6G dye under UV irradiation

N. A. Aziz[a], C. K. Sheng[a,*], H. J. Jie[b]
[a]*Faculty of Science and Marine Environment, Universiti Malaysia Terengganu 21030 Kuala Nerus, Terengganu, Malaysia*
[b]*Atomic M&E Sdn Bhd, 5A, Jalan Seri Orkid 33, Taman Seri Orkid, 81300 Skudai, Johor, Malaysia*

Cubic-phase cadmium sulfide (CdS) nanoparticles were formulated through dropwise precipitation. XRD analysis shows that the CdS has an average nanocrystallite size of approximately 3.36 nm. FTIR results reveals that a strong band appeared around 600 cm^{-1} is due to Cd-S bonds. SEM image demonstrates that many tiny spherical nanoparticles are homogeneously distributed on the sample surface. The CdS nanoparticles show a prominent UV-Vis absorption peak at 506 nm with a direct band gap of 2.24 eV. CdS nanoparticles has induced remarkable photobleaching effect on the highly stable R6G dye solution under UV illumination, which is applicable for future wastewater treatment.

(Received November 16, 2022; Accepted February 9, 2023)

Keyword: CdS nanoparticles, Wastewater treatment, Photocatalytic degradation, Rhodamine 6G, Optical properties

1. Introduction

Recently, a new research field has been developed in the synthesis, characterization and the potential applications of II-IV and III-V group semiconductors that demonstrate unique quantum nano-size effect [1-3]. This is because semiconductor nanostructure, especially those with direct band gap, are widely used in nonlinear optics and optoelectronic devices [4, 5]. Cadmium sulfide (CdS) belongs to II-IV group semiconductors with a direct band-gap of 2.42 eV, and is considered to be one of the most important and promising inorganic materials in various optoelectronic applications, such as light emitting diode, solar panels, electroluminescent, photoluminescent and photoconductive devices [6 - 8]. Also, CdS has been extensively used as a favourable photocatalyst due to its tunable structural and optical properties [9-11]. The band gap width of CdS nanoparticles experiences a remarkable change due to the modifications of size and morphology, hence resulting in significant tunability of optical and photocatalytic properties [12-14]. Numerous methods have been utilized to synthesis the CdS nanoparticles, for instances, vapor deposition [15], biosynthesis [16], laser ablation [17], photochemical [18], precipitation [19, 20], hydrothermal [21] and solvothermal [22, 23] method. Among these methods, precipitation is well recognized as one of the most effective methods for nanoparticle synthesis [19, 20].

Wastewater discharged from industries and households contains many organic compounds known as pollutants [24, 25]. Dye is an example of organic pollutants, consisting of two main groups, chromophores and auxochromes, which can form highly toxic complexes with metal ions in the wastewater and cause severe water pollution [26-28]. Nowadays, environmental problems caused by dye pollution remain an undissolved issue, especially for highly stable commercially available dyes. For example, rhodamine 6G (R6G) is a highly stable laser dye that is very difficult to degrade under normal environment. Also, R6G dye is widely used in textile industry, causing serious pollution to the environment [29-31]. Therefore, in this study, a recognized tool of photocatalytic water remediation is performed to decompose the R6G dye pollutant under UV

* Corresponding author: chankoksheng@umt.edu.my
https://doi.org/10.15251/DJNB.2023.181.203

irradiation by using the CdS nanoparticles as photocatalyst. CdS nanoparticles were synthesized via dropwise precipitation in NaOH solution, and the crystalline structure, functional group, surface morphology, optical and photocatalytic degradation properties of the CdS were elucidated by XRD, FTIR, SEM, UV-Vis spectroscopy, respectively.

2. Materials preparation and characterizations

All chemical reagents were procured from Merck Ltd. and used as received without any special treatment. A dropwise precipitation method was adopted to synthesize the CdS nanoparticles. In the beginning, cadmium chloride ($CdCl_2$) and thiourea (CH_4N_2S) solutions were prepared separately in distilled water at the desirable concentrations, and then both solutions were mixed together to obtain a homogenous solution. Cadmium chloride and thiourea were acted as precursors to produce the Cd^+ and S^- ions for the formation of CdS in aqueous solution. After that, 1.0 M NaOH was dropwisely added to the solution until the colorless solution turned yellow. The solution was then continuously stirred for 1 hour while maintaining the heating temperature at 70 ^oC. The yellow precipitate formed in the solution was filtrated and washed several times with distilled water to remove the impurities and unwanted chemical substances. They were then dried at room temperature for 24 h until the water completely evaporated from the sample. Lastly, the sample was ground into a fine powder and stored in a desiccator prior to characterization. Figure 1 displays a schematic diagram of the preparation procedure of CdS nanoparticles.

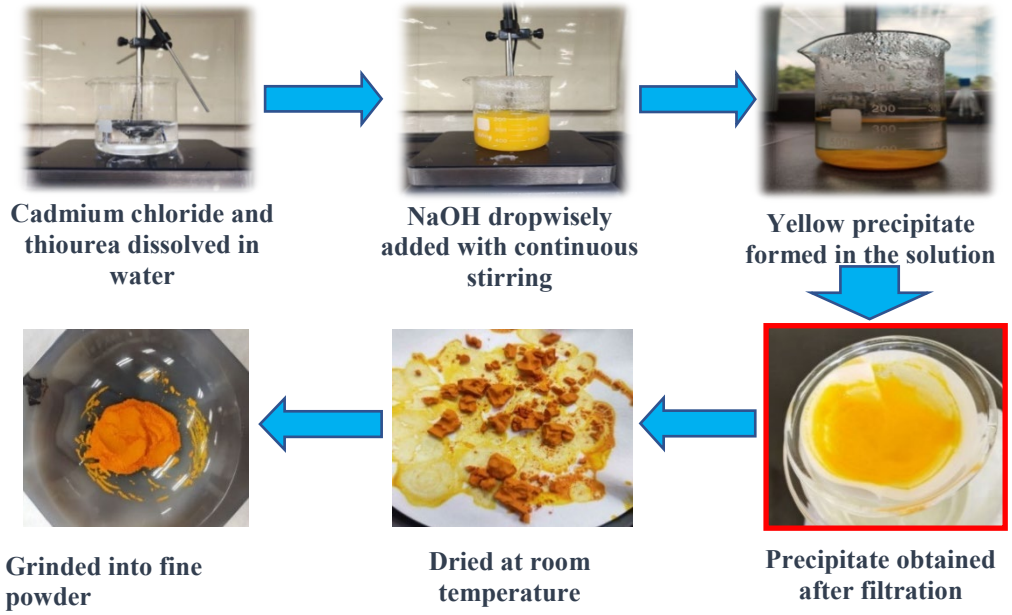

Fig. 1. Preparation procedure of CdS nanoparticles.

The sample underwent characterization by using XRD (Miniflex-TM II) in the range of 2θ = 10 – 80^o to study the crystalline structure. The functional groups of CdS were determined using a Thermo Nicolet Alvatar 380 FTIR in the wavenumber range from 400 cm^{-1} to 4000 cm^{-1}. The UV-Vis absorption spectrum was measured by using a Shimadzu UV-1800 spectrophotometer. The surface morphology of the sample was examined by Tescan Vega SEM. For photocatalytic degradation study, the CdS was added into the R6G dye solution at a concentration of 5 ppm. Next, the mixture was stirred in the dark for 30 minutes in order to achieve an absorption-desorption equilibrium state between dye and catalyst. The solution was then exposed to UV radiation at every 20 minutes time interval until a total irradiation period of 180 minutes was

* Corresponding author: chankoksheng@umt.edu.my

reached. The dye degradation activity was monitored using the UV–Vis spectrophotometer by recording the change of absorption peak at a wavelength of 526 nm. The degradation efficiency (%) was calculated using the following equation,

$$\text{Degradation efficiency (\%)} = (C_o - C_t)/C_o \times 100 \quad (1)$$

in such a way that C_o represents the initial dye concentration and C_t denotes the concentration after irradiation at time t.

3. Results and discussion

Fig. 1 depicts the FTIR spectra of CdS nanoparticles measured within the range of 4000-400 cm^{-1}. The presence of vibrational functional groups in the studied sample can be determined from the bands that emerged in the spectra. From the figure, a broad band situated around 3250 cm^{-1} indicates the vibration of hydroxyl (O–H) stretching, which is ascribed to atmospheric water molecules absorbed on the sample surface [20, 27]. Meanwhile, a moderately sharp peak emerged at 1627 cm^{-1} corresponds to the hydroxyl (O–H) bending vibrational mode [32]. Besides, a sharp band observed at 2358 cm^{-1} is mainly attributed to the surrounding uptake of CO_2 gas molecules adhered to the surface of CdS nanoparticles [33]. Nevertheless, the stretching vibrations of C=O bond [34], C-O bond [34, 35] and C–N bond [35] are found at peak positions of 1740 cm^{-1}, 1375 cm^{-1} and 1215 cm^{-1}, respectively. Significantly, it could be seen that another strong broadband appeared between 540 cm^{-1} and 650 cm^{-1}, which is due to the Cd-S molecular bonding [36]. All vibrational bands positions with related functional groups and the assignments are systematically presented in Table 1.

The XRD pattern of the CdS nanoparticles is presented in Fig. 2. As shown in the figure, three main peaks are observed located at 2θ positions of 26.64°, 44.06° and 52.22° corresponding to (h, k, l) miller indices of (111), (220) and (331) lattice planes. These peaks represent the cubic-phase structure of CdS by referring to JCPDS card number 89-440. The dominant peak is observed on the (111) plane, which indicates the preferential crystallographic orientation of CdS nanoparticles [8]. Furthermore, CdS exhibits highly nanocrystalline feature due to the presence of a broad pattern line of FWHM for each peak. Notably, no other extraordinary peaks are traced in the XRD diffractogram, possibly indicating the high purity of the studied sample [9]. Moreover, the crystallite size is calculated by using the Scherer's equation, $D = k\lambda/\beta\cos\theta$ [10], where k is shape factor with a value of 0.94, λ is the wavelength of radiation emitted from the CuKα source (1.406 nm), β denotes FWHM of the XRD peak and θ represents Bragg's diffraction angle. Thereafter, the lattice strain and the dislocation density of the present sample are further determined, and the obtained related structural parameters are listed in Table 2. Through analysis, the average crystallite size of the CdS nanoparticles is found to be ≈ 3.36 nm as in nano-scale dimension.

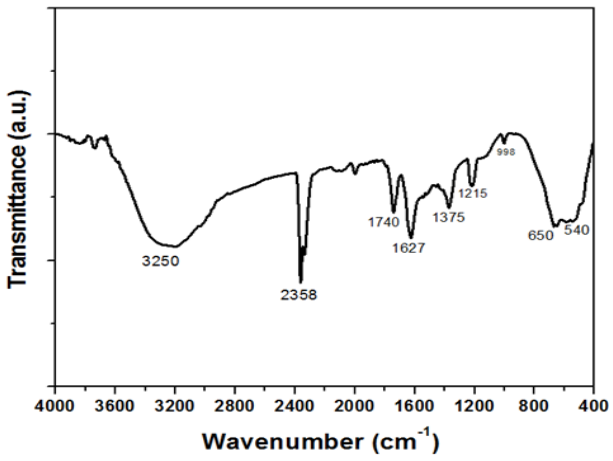

Fig. 1. FTIR spectrum of CdS nanoparticles.

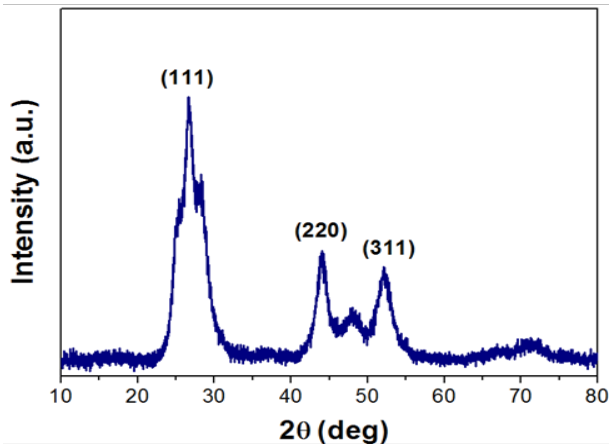

Fig. 2. XRD pattern of CdS nanoparticles.

Table 1. FTIR band assignments and functional groups of CdS nanoparticles.

Position (cm^{-1})	**Assignment**	**Functional group**	**Intensity**	**Ref.**
3250	hydroxyl (O–H) stretching vibration	Alcohols phenols	Broad	[20, 35]
2358	vibrational CO_2	Carbon dioxide	Sharp	[33]
1740	stretching vibrations of C=O	Carbonyl	Small	[34]
1627	hydroxyl (O–H) bending vibration	Alkyl halides	Medium	[32]
1375	stretching vibrations of C-O bonds	Phenol	Small	[34, 35]
1215	C–N Stretching vibration	Aromatic amines	Small	[35]
650	Cd-S bond	Metal sulfide	Strong	[11, 36]

Table 2. Structural parameters obtained for the present CdS nanoparticles.

Peak position (2θ)	**Plane (h,k,l)**	**FWHM (deg)**	**Crystallite size, D (nm)**	**Micro strain, ε ($\times 10^{-3}$)**	**Dislocation density, δ ($\times 10^{-3}$ nm^{-2})**
26.64°	(111)	3.54	2.41	65.19	172.17
44.06°	(220)	1.82	4.92	19.63	41.31
52.22°	(331)	3.22	2.87	28.71	121.41

The surface morphology was further examined by exploiting the SEM imaging analysis. Fig. 3 (a) shows the SEM image of CdS, while Fig. 3 (b) exhibits the histogram of the particle size distribution. From the figure, a well-defined structure is observed, since many small spherical-shaped nanoparticles are uniformly distributed on the sample surface. The average particle size was determined to be in the range of about 80 - 100 nm. The smaller nano-sized particles ascertained may cause an increase in surface area and grain boundaries, which are beneficial for charge carrier transitions during the photocatalytic activity. Also, it can be seen that some larger particles are outgrown from the structure surface owing to the coalescence of the nanoparticles, indicating that every single particle might consist of many small nanocrystallites, as validated from the XRD analysis.

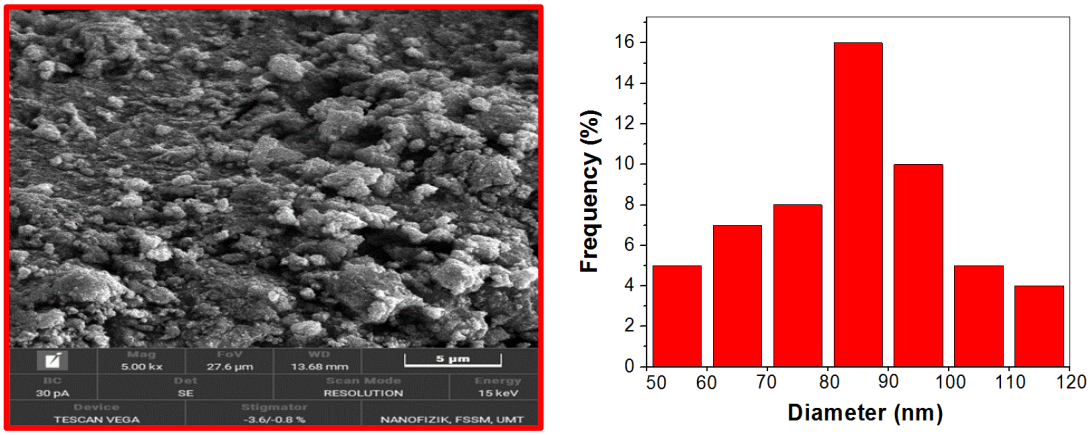

(a) *(b)*

Fig. 3. (a) SEM image of CdS nanoparticles and (b) particle size distribution.

The optical absorption spectra were recorded at room temperature using the UV-Visible spectrophotometer. Fig. 4(a) illustrates the absorption spectra of CdS nanoparticles over a visible wavelength region of 400 nm to 800 nm. From the spectra, the CdS exhibits a prominent absorption peak at 506 nm. This result indicates that partially hydrophilic nature of CdS is formed in the aqueous solution due to a better dissolubility of the nanoparticles with a large number of O-H functional groups attached to the surface, which has been evidenced from the FTIR analysis. Another possible explanation could be related to the existence of extremely small nanoparticles that easily dissolve in the water. Afterwards, the optical band gap was evaluated from the Tauc's relation as given by [11, 20, 32]:

$$(\alpha h\upsilon) = B\,(h\upsilon - E_g)^{n} \tag{2}$$

where α represents the optical absorption coefficient, h is the Planck's constant, υ is the radiation frequency, B is a proportionality constant, E_g denotes the band gap value and the n designates the type of electronic transition. In this study, n would take a value of 1/2, since the CdS is literally assigned to a direct band gap semiconductor. Fig. 4(b) shows the plot of $(\alpha h\nu)^2$ versus photon energy for the CdS nanoparticles [5, 23]. As demonstrated in the figure, a linear straight line was fitted and extended for an intersection with photon energy ($h\nu$) axis.

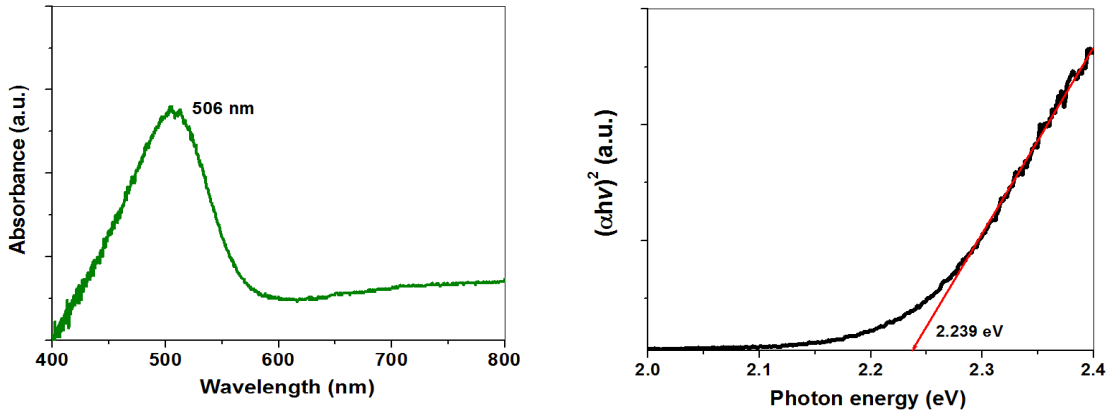

Fig. 4. (a) UV-visible optical absorption spectra and (b) $(\alpha h\nu)^2$ versus photon energy of the CdS nanoparticles.

From the intercepted point, the band gap value is determined to be 2.239 eV, which is slightly narrower as compared to the reported literature value of bulk CdS (~2.42 eV). This feature may assist to increase the rate of photo-induced charge carrier transition and in turn enhance the photocatalytic activity. As reported by Solanki et al. [36], the shrinkage of the band gap for a nanomaterial can be influenced by increasing the crystallite size.

The obtained CdS nanoparticles were utilized as photocatalyst to study the degradation of R6g in an aqueous solution as the model dye for water pollution remediation. Fig. 5(a) displays the variation of UV-visible spectrum with respect to irradiation time. As can be seen from the figure, the main absorption peak of R6G dye solution positioned at 526 nm shows a gradual decay as the progress of irradiation time. This remarkable reduction in absorbance means that continual UV light illumination has initiated a notable photodecolouration effect on R6G dye molecules, a very photostable dye used in textiles and laser products. Figure 5(b) shows the degradation percentage versus the irradiation time. From the figure, it could be observed that the degradation percentage increases with irradiation time. Clearly, the plot shows a steeper slope for the first 20 minutes owing to a faster dye degradation rate. Afterwards, the dye degradation takes place slowly throughout the entire process. The result shows that the degradation efficiency achieved is 24.68 % after 180 minutes irradiation under the UV light. This finding implies that the combination of UV light and CdS photocatalyst contribute to an appreciable improvement on the R6G degradation at prolonged exposure duration. Figure 5(c) and 5(d) show the plots of C/C_o and $\ln(C/C_o)$ against irradiation time, respectively. The photocatalytic degradation of R6G obeys pseudo first-order reaction kinetics [31-35]. This is because a linear relationship is obtained from the plot of $\ln(C/C_o)$ versus irradiation time, as depicted in Figure 5(d). Using pseudo-first-order kinetics, the corresponding rate constant is calculated to be 0.0127 min^{-1} with a high correlation coefficient of R = 0.9618 via equation (2):

$$\ln (C/C_o) = -kt \tag{3}$$

where C_o designates the initial aqueous dye concentration, C denotes dye concentration at any time intervals, t and k represent the 1st order kinetic rate constant.

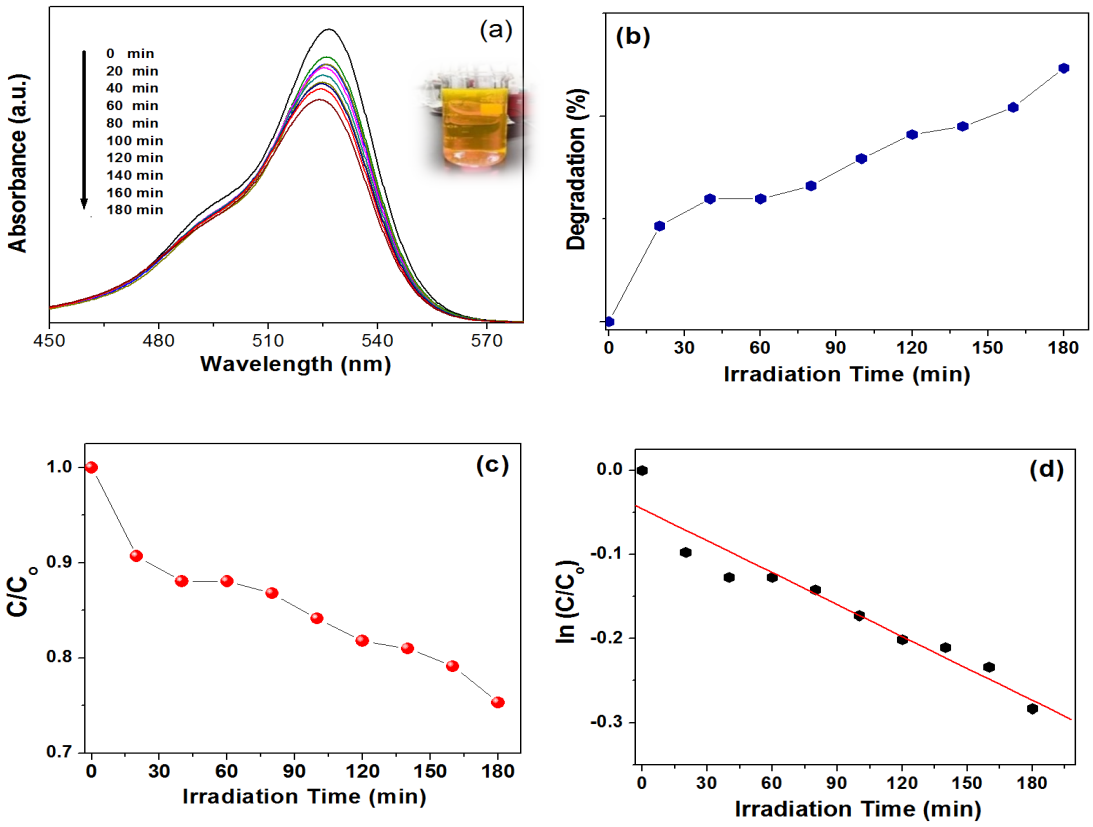

Fig. 5. (a) Variation of absorption spectra of R6G under UV irradiation; (b) percentage of degradation with irradiation time; (c) degradation curve of C/C_o versus time and (d) first-order kinetics fitting of $\ln(C/C_o)$ versus time for R6G degradation.

The obtained kinetic value further validates that the presence of CdS nanoparticles as photocatalysts can provide an active site for the photodecolorization of R6G dye, since the dye degradation is ineffective in the absence of catalyst. In addition, the main factor for the R6G dye degradation to occur can be ascribed to the generation and separation of photo-induced electron-hole pairs due to the absorption of sufficient incident photon to overcome the bandgap barrier. When the CdS catalyst is exposed to UV light, the photon energy will be absorbed by the studied catalyst, and hence resulting in the generation of electron-hole pairs. The electron-hole pairs will then react with O_2 and H_2O to produce the free radicals, which will eventually decompose the R6G dye molecules into harmless species [18]. Nevertheless, according to Prabu et al. [35], the degradation efficiency can be further improved by applying larger amount of photocatalyst or higher power of UV light.

5. Conclusion

In the present investigation, CdS nanoparticles have been successfully synthesized through dropwise precipitation. According to XRD pattern analysis, CdS demonstrates a crystalline cubic structure, and the average crystallite size is determined to be around 3.36 nm. In the FTIR spectrum, it shows that a dominant broad band appeared in the range of 540 − 650 cm^{-1} can literately represent the Cd-S stretching bond. CdS also exhibits a well-defined surface structure, whereby tremendous spherical nanoparticles with size ranging from 80 to 100 nm are evenly distributed on the sample surface. This CdS demonstrates a prominent absorption peak at 506 nm with a band gap of 2.24 eV determined by the Tauc's relation. Under UV irradiation, CdS successfully degrades the yellowish-range Rhodamine 6G dye with a degradation efficiency of 24.68 %. This finding further confirms that CdS can potentially be applied as an efficient photocatalyst in future water remediation process.

Acknowledgements

The authors would like to acknowledge the Universiti Malaysia Terengganu and the Malaysian Government for the financial assistance in accomplishing this research through the research grant (TAPE-RG-55290).

References

[1] M. S. Almomani, N. M. Ahmed, M. Rashid, M. A. Almessiere, A. S. Altowyan, Mater. Chem. Phys. 258, 123935 (2021); https://doi.org/10.1016/j.matchemphys.2020.123935

[2] H. Dang, E. Ososanaya, N. Zhang, Opt. Mater. 132, 112721 (2022); https://doi.org/10.1016/j.optmat.2022.112721

[3] M. Fatolah, G. Khayati, P. Fatolah, J. Sulphur Chem. 43, 366 (2022); https://doi.org/10.1080/17415993.2022.2052883

[4] C. K. Sheng, M. G. M. Sabri, M. F. Hassan, E. A. G. E. Ali, Dig. J. Nanomater. Biostructures. 16, 1379 (2021).

[5] R. Ariff, C. K. Sheng, Dig. J. Nanomater. Biostructures. 16, 809 (2021).

[6] N. S. Priya, S. S. P. Kamala, V. Anbarasu, S. A. Azhagan, R. Saravanakumar, Mater. Lett. 220, 161 (2018); https://doi.org/10.1016/j.matlet.2018.03.009

[7] A. Abdel-Galil, H. E. Ali, M. R. Balboul, Optik 129, 153 (2017); https://doi.org/10.1016/j.ijleo.2016.10.061

[8] C. K. Sheng, K. A. M. Amin, L. L. Hong, M. F. Hassan, M. Ismail, Int. J. Electrochem. Sci. 12, 10023 (2017); https://doi.org/10.20964/2017.11.75

[9] M. Shkir, K. V. Chandekar, A. Khan, A. Mohamed El-Toni, I. M. Ashraf, M. Benghanem, S. F. Adil, A. A. Ansari, H. Ghaithan, S. AlFaify, Mater. Chem. Phys. 255, 123615 (2020);

https://doi.org/10.1016/j.matchemphys.2020.123615
[10] V. H. Martínez-Landeros, N. Hernandez-Como, G. Gutierrez-Heredia, M. A. Quevedo-Lopez, F. S. Aguirre-Tostado, Thin Solid Films 682, 24 (2019); https://doi.org/10.1016/j.tsf.2019.05.014
[11] C. K. Sheng, Y. M. Alrababah, Kuwait J. Sci. 49, 1 (2022); https://doi.org/10.48129/kjs.11913
[12] N. Saxenaa, T. Kalsib, P. Uttamb, P. Kumarb, Opt. Mater. 84, 625 (2018).
[13] X. Yang, Y. Yang, B. Wang, T. Wang, Y. Wang, D. Meng, Solid State Sci. 92, 31 (2019); https://doi.org/10.1016/j.solidstatesciences.2019.04.004
[14] C. K. Sheng, Y. M. Alrababah, J. Nano- Electron. Phys. 12, 01017 (2020); https://doi.org/10.21272/jnep.12(1).01017
[15] L. Huang, Z. L.Wei, F. M.Zhang, X. S. Wu, J. Alloys Compd. 648, 591 (2015); https://doi.org/10.1016/j.jallcom.2015.07.041
[16] S. A. E. Moghaddam, P. Ghadam, F. Rahimzadeh, J. Clean. Prod. 356, 131848 (2022); https://doi.org/10.1016/j.jclepro.2022.131848
[17] A. A. Lalayan, Appl. Surf. Sci. 248, 209 (2005); https://doi.org/10.1016/j.apsusc.2005.03.004
[18] M. Marandi, N. Taghavinia, A. Iraji, S. M. Mahadavi, Nanotechnology 16, 334 (2005); https://doi.org/10.1088/0957-4484/16/2/027
[19] Y. M. Alrababah, C. K. Sheng, M. F. Hassan, Chalcogenide Lett. 16, 297 (2019).
[20] Y. M. Alrababah, C. K. Sheng, M. F. Hassan, Nano-Struct. Nano-Objects 19, 10034 (2019); https://doi.org/10.1016/j.nanoso.2019.100344
[21] Z. Jinxin, Z. Gaoling, H. Gaorong, Front. Chem. China 2, 98 (2007).
[22] M. R. M. Dris, C. K. Sheng, M. I. N. Isa, M. H. Razali, Int. J. Tech. 1, 1 (2012).
[23] M. R. M. Dris, M. I. N. Isa, M. Ismail, C. K. Sheng, Int. J. Electroact. Mater. 1, 23 (2013).
[24] N. Venkatesh, K. Sabarish, G. Murugadoss, R. Thangamuthu, P. Sakthivel, Environ. Sci. Pollut. Res. 27, 43212 (2020); https://doi.org/10.1007/s11356-020-10268-3
[25] E. Bruno, M. Haris, A. Mohan, M. Senthilkumar, Appl. Phys. A. 127, 1 (2021); https://doi.org/10.1007/s00339-021-05081-9
[26] W. M. M. Yunus, K. S. Chan, W. M. Z. W. Yunus, J. Nonlinear Opt. Phys. Mater. 12, 91 (2003); https://doi.org/10.1142/S0218863503001237
[27] K. S. Chan, W. M. M. Yunus, Pertanika J. Sci. Technol. 13, 23 (2005); https://doi.org/10.1007/s10550-005-0003-8
[28] M. F. A. Aziz, N. L. A. Wahab, K. S. Chan, Mal. J. Microsc. 7, 109 (2011).
[29] A. M. Asiri, M. S. Al-Amoudi, T. A. Al-Talhi, A. D. Al-Talhi, J. Saudi Chem. Soc. 15, 121 (2011); https://doi.org/10.1016/j.jscs.2010.06.005
[30] E. Pino, C. Calderón, F. Herrera, G. Cifuentes, G. Arteaga, Front. Chem. 8, 1 (2020); https://doi.org/10.3389/fchem.2020.00365
[31] T. K. Ghorai, N. Biswas, J. Mater. Res. Technol. 2, 10 (2013).
[32] F. Soleimani, A. Nezamzadeh-Ejhieh, J. Mater. Res. Technol. 9, 16237 (2020); https://doi.org/10.1016/j.jmrt.2020.11.091
[33] M. An, L. Li, X. Gao, Y. Zhu, J. Guan, Q. Wu, Colloids Surf. A Physicochem. Eng. 643, 128794 (2022); https://doi.org/10.1016/j.colsurfa.2022.128794
[34] D. Das, P. Nandi, Appl. Surf. Sci. 570, 151260 (2021); https://doi.org/10.1016/j.apsusc.2021.151260
[35] H. J. Prabu, R. Varghese, I. Johnson, S. J. Sundaram, A. D. Raj, R. Rajagopal, P. Kuppusamy, R. Sathya, K. Kaviyarasu, Environ. Res. 212, 113295 (2022); https://doi.org/10.1016/j.envres.2022.113295
[36] R. G. Solanki, P. Rajaram, Nano-Struct. Nano-Objects 12, 157 (2017); https://doi.org/10.1016/j.nanoso.2017.10.003